# REDUCING THE ERROR IN TERRESTRIAL LASER SCANNING BY OPTIMIZING THE MEASUREMENT SET-UP

**Sylvie Soudarissanane, Roderik Lindenbergh and Ben Gorte**

Delft Institute of Earth Observation and Space Systems(DEOS)
Delft University of Technology
Kluyverweg 1, 2629 HS Delft, The Netherlands
(S.S.Soudarissanane, R.C.Lindenbergh, B.G.H.Gorte)@tudelft.nl
http://www.deos.tudelft.nl/

**Commission WG V/3**

**KEY WORDS:** Laser scanning, point cloud, error, noise level, accuracy, optimal stand-point

**ABSTRACT:**

High spatial resolution and fast capturing possibilities make 3D terrestrial laser scanners widely used in engineering applications and cultural heritage recording. Phase based laser scanners can measure distances to object surfaces with a precision in the order of a few millimeters at ranges between 1 and 80 m. However, the quality of a laser scanner end-product, like a 3D model, is influenced by many different parameters, especially the relative object surface orientation and the local point cloud density. This paper introduces the notion of point cloud quality. The obtained point cloud is first segmented using a planar feature extraction segmentation. Each segment is subdivided into smaller patches of $20 \times 20$ cm. For each patch a patch quality parameter is determined, which incorporates the local point density and local point quality. By averaging the patch quality over the complete point cloud, a point cloud quality is derived. This paper demonstrates this approach in practice by comparing two scans of the same test room obtained from different stand-points. As a result, it is shown and analyzed that by simply moving the scanner by two meters, the quality of the point cloud can be improved by 25 %.

## 1 INTRODUCTION

The terrestrial laser scanning technology is increasingly being used for representing and analyzing 3D objects in a wide range of engineering applications. One of the main applications of the terrestrial laser scanner is the visualization, modeling and monitoring of man made structures like buildings. Especially surveying applications require on one hand a quickly obtainable, high resolution point cloud but also need observations with a known and well described quality. The phase based measurement technique, where the phase of a multi-modulated wave determines the distance to an object, is used in recent years mainly because of its high speed. A complete quality description of individual scan points is still under active research. However, major error components have already been identified. In this paper, it is shown how an analysis of the individual point quality and local point density can be exploited to improve the measurement set up.

A laser scan provides a spherical representation of the surroundings with the center of the scanner as the origin of a local coordinate system. It uses the reflection of the laser beam on the object surface to acquire a range measurement as well as an intensity value of the reflected light. The accuracy of the range measurement is dependant on four main parameters:

- Scanner mechanism precision, e.g. mirror center offset, rotation mechanism abberations (Lichti, 2007, Li and Mitchell, 1995, Zhuang and Roth, 1995).
- Properties of the scanned surface, e.g. roughness, reflectivity, color (Bucksch et al., 2007, Křemen et al., 2006, Clark and Robson, 2004).
- Conditions of the experiment environment, e.g. ambient light, humidity, temperature (Pfeifer et al., 2007, Lichti and Gordon, 2004, Böhler et al., 2003).
- Scanning geometry, e.g. incidence angle on the surface, range differences (Böhler et al., 2003, Cheok et al., 2002, Soudarissanane et al., 2007).

To obtain a 3D point cloud, the scene is scanned from different positions around the considered object. The scanning geometry plays an important role in the quality of the resulting point cloud. Errors due to the scanning geometry are relatively well-described. The ideal set-up for scanning a surface of an object is to position the laser scanner in such a way that the laser beam is near perpendicular to the surface. Due to scanning conditions, such an ideal set-up is in practice not possible. The different incidence angles and ranges of the laser beam on the surface result in 3D points of varying quality. Here we define the incidence angle as the angle between that surface normal that is pointing in the surface, and the incoming laser beam direction. The following two correlated components variate with respect to the scanning geometry:

- Range quality. The study of the quality of range measurements as a function of the scan angle has proven that in general the lower the incidence angle and the lower the range, the higher the accuracy of the range distance measurement. (Soudarissanane et al., 2007)
- Point cloud density. The density of the point cloud decreases with increasing incidence angles and range (Lindenbergh et al., 2005).

Usually the scene is scanned from several positions around the area of interest. The position or stand-point of the scanner that gives the best accuracy, in terms of Least Mean Square Error (Teunissen, 1991), is generally not known. Using the optimal stand-point of the laser scanner on a scene will improve the quality of individual point measurements and the overall local redundancy of the measurements. This paper deals with the design of a measurement setup by showing how the stand-point of the laser scanner influences the point cloud quality.

## 2 METHODOLOGY

The quality analysis of the point cloud is described using the error propagation techniques. The point cloud is first segmented

based on a planar feature extraction algorithm. Using the Principal Component Analysis, the planar parameters of each segments are estimated. Each segments are then subdivided into smaller areas, which are called in this paper patches. The quality of each patch is described using a Least Square Estimation.

### 2.1 Segmentation

Segmentation algorithms group points that have similar properties under a given homogeneity criterion. Although architecture uses many surface types, planar surfaces are prominent in most of human made objects. In this paper, the planar surfaces are extracted using a gradient based range image (Gorte, 2007). This method estimates, for each measurement, two angles $(\theta, \varphi)$ and the distance $(\rho)$ between the plane the measurement belongs to and the origin. This estimation is based on the scan parameters and horizontal and vertical gradient images. Regions with similar planar parameters $(\theta, \varphi, \rho)$ are considered to be part of the same plane, i.e. segment. For the experiments presented in this paper, small segments are filtered out from the analysis. Note that this segmentation is based on the range image and therefore does not take into account the intensity measurements.

### 2.2 Patch subdivision

To have a better insight into the local error behavior and the local quality of points of similar scanning geometry, each segment is subdivided into small patches of $20 \times 20$ cm.

### 2.3 Data representation

3D laser scans can be seen as panoramic images, such as the one depicted in Fig.1(a). In this study, planar features of the area are extracted and studied. In order to have a better and easier visualization of the experimental results, the point cloud is represented as a net view. Fig. 1(c) shows a model of a net view. This type of view allows a real $2.5$D visualization of the scene in such a way that the relative scale is maintained. In the rest of the paper, signal variations are considered perpendicular to the planar segments.

### 2.4 Point density

A point cloud consists of a spherical representation of the surroundings, the center of the laser scanner for origin. It provides a horizontal angular position $\alpha$, a vertical angular position $\beta$ and a range measurement $\gamma$. The point cloud density depends on the scan parameters, i.e. the angular resolution, but also on the scanning geometry, i.e. the incidence angle and the distance of the object. The point density decreases with increasing range and increasing incidence angle (Lindenbergh et al., 2005). In this paper, the local point density is incorporated in the description of the local point cloud quality by considering the relative redundancy in determining local patch parameters.

### 2.5 Incidence angle

The incidence angle $i$ is defined as the angle between the laser beam and the normal of the considered surface. It is known that the object surface orientation influences the quality of the point cloud data, e.g. (Soudarissanane et al., 2007). In this paper, the influence of the incidence angle on the local point cloud quality is indirectly incorporated by considering the local noise levels when determining local patch parameters.

### 2.6 Principal Component Analysis

A commonly used planar fitting algorithm is the ordinary Least-Squares analysis. However, for an important amount of dataset, the main drawback of the Least-Squares analysis lies on the amount of memory needed. Instead, the Principal Component Analysis (PCA) is used on the segments. The linear regression determined by a PCA minimizes the perpendicular distances from the point cloud to the fitted model (Lay, 2002). The PCA is comparable to a Total Least-Squares method (Teunissen, 1991), known to be robust to outliers and fast computing. The PCA method determines the optimum basis, in terms of Least-Mean-Squares-Error, in which the data set can be re-expressed, using orthogonal linear transformations.

**Principle** Consider the set of $n$ points $X = [x_i, y_i, z_i]_{i=1,\ldots,n}$ that belong to measurements of a planar surface. As described in Eq.1, the aim is to find the basis $B$ that transforms the original data $X$ into $Y$. The basis $B$ estimates the best plane that minimizes the perpendicular distances from the data to the fitted model.

$$Y = B \cdot X \tag{1}$$

*Step 1* - The point cloud is first centered around its center of gravity $M$ so that the data set has a zero empirical mean.
*Step 2* - The covariance matrix $C_X$ of the centered data is computed as defined in Eq.2.

$$C_X = \frac{1}{n-1} X X^T \tag{2}$$

*Step 3* - The eigenvectors $V$ of the covariance matrix $C_X$ and the diagonal matrix of the eigenvalues of the covariance matrix $C_X$ are computed as in Eq.3

$$V^{-1} C_X V = D \tag{3}$$

*Step 4* - The two eigenvectors corresponding to the two highest eigenvalues represent the two 2D axes of the fitted model. The third eigenvector, which corresponds to the lowest eigenvalue, is orthogonal to the first two and defines the normal vector $\overrightarrow{N}$ of the plane.

### 2.7 Error Modeling and quality of the planar patch

In ordinary Least-Squares analysis (Teunissen, 1991), the linear model that fits the best the experimental dataset is computed. The model minimizes the Euclidian norm of the residuals. The error is measured as the squared distance from the data to the fitted function, along a particular axis of direction. This modeling technique is not robust for noisy data and the solution provided is not necessarily the optimal one. Instead, the solution provided by an orthogonal optimization is more suitable to noisy data.
Let $M = (M_x, M_y, M_z)$ the center of gravity of the dataset. The error $\hat{e}$ modeled in Eq.4 for each individual point $(x_i, y_i, z_i)$ is the orthogonal squared distance from the point to the fitted function.

$$\hat{e} = |(x_i - M_x, y_i - M_y, z_i - M_z) \cdot \overrightarrow{N}|_{i=1,\ldots,n} \tag{4}$$

For each patch, the Root Mean Squared Error (RMSE) $\sigma_{\hat{e}}$ is computed as described in Eq.5, from which the matrix of observational variances $Q_{\hat{y}}$ is derived as shown in Eq.6

$$\sigma_{\hat{e}} = \sqrt{\frac{\hat{e}^T \hat{e}}{n}} \tag{5}$$

$$Q_{\hat{y}} = \sigma_{\hat{e}} \cdot I_n \tag{6}$$

Incorporating the $\sigma_{\hat{e}}$ means that the local noise level is used to express confidence in how well the local patch points determine

the local patch parameters. In this paper, the point cloud is represented as a net view, therefore, the only planar parameter quality to be estimated is the height $z$ of the point with respect to the planar fitting. Assume the following linear model: $Z = A \cdot P$, where $A = [x_i, y_i, 1]_{i=1,\ldots,n}$, $Z = [z_i]_{i=1,\ldots,n}$ and $P$ represents the planar patch parameters. The variance-covariance matrix of the planar patch parameters is given in Eq.7

$$Q_{\hat{p}} = A^T Q_{\hat{y}}^{-1} A \tag{7}$$

In determining the local patch parameters, a higher number of local patch points will result in more accurate local patch parameters. In general, using the redundancy of the observations allows to derive adjusted points on the adjusted local planar patch with a precision far below the nominal point precision of an individual laser point. For each set of points $X$, the propagated variance $\hat{\sigma}_m$ at the center of gravity $M$ is considered as shown in Eq.8.

$$\hat{\sigma}_m = A_m^T Q_{\hat{p}}^{-1} A_m \tag{8}$$

where $A_m = [M_x, M_y, 1]$.

## 3 EXPERIMENT SET-UP

The laser scanner measurements optimization is investigated using the experiment set-up as shown in Figure 1. The laser scanner LS880 HE80 from FARO (FARO, 2007) is used. The laser beam of this laser scanner is deflected at $90^o$ on a rotating mirror which determines the vertical field of view of $320^o$ since the scanner cannot scan under itself. The head of the scanner rotates around its vertical axis to allow the horizontal field of view of $360^o$. A full resolution scan has typically around 130 million of points. The experiments are performed in a closed area with short ranges, therefore the temperature and humidity influences are neglected. The scans considered here contain about 26 millions of points.

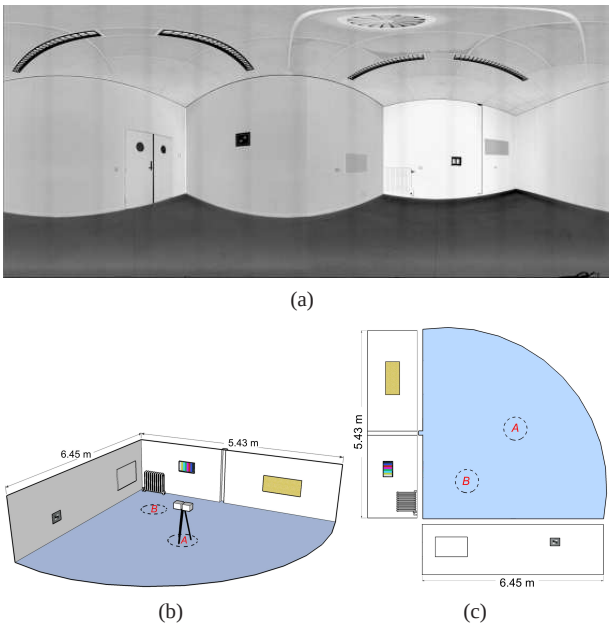
The room scanned for this experiment consists of two planar walls and one cylindric wall. As the focus of this paper is into the planar features quality, the cylindric wall is excluded from the analysis. As depicted in Fig.1(a), the laser scanner provides a panoramic view of the area by measuring the reflection of a phase modulated laser beam. The laser scanner cannot scan shiny materials such as metal or mirror like materials, and low reflectance materials are measured with lower accuracies (Bucksch et al., 2007, Křemen et al., 2006, Clark and Robson, 2004). The ceiling of the room of experiment contains very shiny materials and is composed of several small segments. Therefore, the ceiling is not part of this study. The floor is covered with light colored linoleum. The walls are painted in white and are very smooth surfaces.

Four test plates that were used in previous studies are added on the two planar walls. Two reference charts (ESSER TE 106 and TE 109) for color and grey scale were previously used in a remission experiment (Bucksch et al., 2007). A white coated plywood and a medium-density fibre board were used before in a scan angle experiment (Soudarissanane et al., 2007). Fig.1(b) represents a 3D model of the room of experiment.

The laser scanner scans the room from two different stand-points. The stand-point $A$ is approximately situated in the middle of the room. The stand-point $B$ is situated in the corner formed by the two planar walls.

## 4 RESULTS AND DISCUSSION

In this section, the influence of the location of the laser scanner on the point cloud quality is presented, based on two stand-points.




(a) (b) (c)

Figure 1: **(a)** Panoramic intensity image obtained with the FARO LS880 laser scanner, **(b)** 3D view model of the experiment set-up, **(c)** Net model of the room of experiment, A and B are two stand points of the laser scanner.

### 4.1 Intensity measurements

In addition to the cartesian coordinates, for each point in the point cloud an intensity value ranging from 0 to 1 is given. This intensity value represents the amount of reflected light intensity as regard to the emitted light. This value is provided by the manufacturer of the laser scanner. According to the providers, the laser scanner measure the received intensity value, which depends on the surface roughness, but also on the scattering behavior of the surface based on its reflectivity properties. Note that this product is not calibrated. Fig.2 depicts the point cloud colored with the measured intensity value for both stand-points. As the laser scanner cannot scan under itself, an empty spot is observed at the position of the laser scanner.

The intensity values on the walls at the position $A$, shown in Fig.2(a) are homogeneous for each scanned surface. The distances to each surface are large enough to obtain homogeneous intensity values. The walls are painted in white, which has high reflectance properties. The returned signals are stronger for the white walls than for the light-colored floor reflections. The wooden plate hang on the upper left wall as depicted in Fig.2(a). It has lower reflectance properties than the white walls or the white plate, therefore has lower measured intensity values. The two reference charts are having a black-colored frame with a very low reflectance property.

Fig.2(b) shows the intensity measurements from position $B$, where the laser scanner was placed nearer to the corner formed by the two planar walls. A saturation effect is observed for signals obtained with near perpendicular scanning direction. The white walls and the light-colored floor have a similar order of intensity values. At the near perpendicular directions, the saturation is characterized by very high intensity values. The spatial intensity distribution is clearly affected by the position of the scanner.

### 4.2 Incidence angles

Fig.3 depicts the incidence angle of the laser beam for each stand-points. Clearly the position of the laser scanner has an influence

on the local incidence angle. Angles plotted in red may indicate scan points of less accuracy. It is clearly seen that for large incidence angles, the point cloud density decreases. Note that at larger incident angles ($i > 60^\circ$), the intensity measurements for the wooden plate and the test charts are distorted, relative to the stand-point $A$ intensity measurements (Fig.2(a)). This effect is due to bigger footprints for high incidence angles.

### 4.3 Segmentation

Fig.4 depicts the segmentation result for both stand-points. The room is segmented into eight main segments. As depicted in Fig.4, at larger incident angles ($i > 60^\circ$), the wooden plate segments and the lower wall test chart segment are distorted and bigger, when comparing to the stand-point $A$ segmentation (Fig.2(a)). This example clearly demonstrates that changing local point quality has immediate effects on post-processing, like in this case segmentation.

### 4.4 Individual point residual of a planar fitting

For each segment, a plane is fitted according to the method described in Sec.2.6. Fig.5 shows the residual $\hat{e}$ for each point of each segment of the point cloud. The points colored in magenta represent residuals higher than 2 cm. Fig.5 shows the individual point residual for the stand point $A$. The estimated planes for both walls produce very low residuals ($< 1$ cm). The points on the floor segment that are situated in high incidence angle areas produce high residuals. By moving the scanner from the stand-point $A$ to the stand-point $B$, high incidence angles at the bottom left corner of segment 1 are avoided. In white, the RMSE per segment is plotted. The differences in RMSE between stand-point $A$ and $B$ can partially be explained by comparing the different incidence angle pattern for each segment. Note that in the stand-point $B$ results, a stripe can be observed in segment 1, corresponding to the $0 = 360^\circ$ transition of the horizontal scan angle. A possible explanation for this effect can be found in saturation: in Fig.2(b), a saturation effect is observed at the near perpendicular surfaces to the laser beam. The points measured shortly after the saturation are all affected by a higher residual. This effect can be explained by an overload of the intensity sensor of the laser beam.

### 4.5 Patch point density

In Fig.6, the number of points per patch of $20 \times 20$ cm is shown. In general, the scanner position at the stand-point $B$ results in a higher point density. For both positions, the point density decreases rapidly with range and with increasing incidence angle. This holds especially towards the far sides of the segments.

### 4.6 Planar patch quality

Each segment is subdivided into small patches of $20 \times 20$ cm. From the points in the patch, local planar parameters are determined as described in section 2.7. The quality of the local patch is evaluated by one number: the standard deviation in the direction perpendicular to the local patch of the center of gravity of the points belonging to the patch. This standard deviation $\hat{\sigma}_m$ is determined according to Eq.8. Clearly this standard deviation reflects both the individual point quality, compare Fig.5, and the local point density, compare Fig. 6. In Fig.6 the mean of the patch variances for each of the four largest segments is plotted in white. On average, the position in the corner (stand-point$B$) results in patches of better quality. The average patch variance for all patches together equals $0.0023$ m for the stand-point $A$ and 0.0017 m for the stand-point $B$. This shows that by simply moving the scanner by two meters, the quality of the point could can be improved by 25 %.

## 5 CONCLUSIONS AND FUTURE WORK

It is well-known that the position of the scanner affects the quality of individual scan points. In this paper, we were able to actually quantify this effect by introducing a notion of point cloud quality, that incorporates both the point density and the individual point quality. It is shown that by moving a scanner by an ample 2 meters, the point cloud quality can be improved by 25 %.

In a next step the optimal scanner position could be determined by using error models from the major error components, like the scanning geometry, the material properties, the scanner mechanism and the environmental conditions. For a complex scene, first a small resolution sketch scan could be used to determine the optimal measurement setup. To proceed in this direction a thorough knowledge of all the error components is preferable, meanwhile use can be made of well described parameters like the incidence or the point density.

## REFERENCES


Böhler, W., Bordas Vicent, M. and Marbs, A., 2003. Investigating Laser Scanner Accuracy. In: CIPA 2003 XVIII International Symposium, Vol. XXXIV(5/C15), Antalya,Turkey, pp. 696–701.

Bucksch, A., Lindenbergh, R. and van Ree, J., 2007. Error budget of Terrestrial Laserscanning: Influence of the intensity remission on the scan quality. In: Proceedings GeoSiberia, Novosibirsk, Russia.

Cheok, G. S., Leigh, S., and Rukhin, A., 2002. Technical report: Calibration Experiments of a Laser Scanner. National Institute of Standards and Technology.

Clark, J. and Robson, S., 2004. Accuracy of Measurements made with a CYRAX 2500 Laser Scanner Against Surfaces of Known Colour. In: XXth ISPRS Congress, Geo-Imagery Bridging Continents, Vol. XXXV(B5), Istanbul, Turkey, pp. 1031–1036.

FARO, 2007. Laser Scanner LS 880 Techsheet. Accessed September 2007, http://www.faro.com/.

Gorte, B., 2007. Planar Feature Extraction in Terrestrial Laser Scans using Gradient Based Range Image Segmentation. In: Proceedings of the ISPRS Workshop, Laser Scanning 2007 and SilviLaser 2007, Vol. XXXVI(3/W52), Espoo, Finland, pp. 173–177.

Křemen, T., Koska, B. and Pospíšil, J., 2006. Verification of Laser Scanning Systems Quality. In: Proceedings XXIII FIG Congress, Munich, Germany.

Lay, D. C., 2002. Linear Algebra and Its Applications (3rd edition). Addison-Wesley.

Li, W. X. and Mitchell, L. D., 1995. Laser scanning system testing–Errors and improvements. Measurement 16(2), pp. 91–101.

Lichti, D., 2007. Error modelling, calibration and analysis of an AM-CW terrestrial laser scanner system. Vol. 61-5, pp. 307–324.

Lichti, D. and Gordon, S., 2004. Error propagation in directly georeferenced Terrestrial Laser Scanner point clouds for cultural heritage recording. In: Proceedings FIG WSA Modelling and Visualization, Athens, Greece.

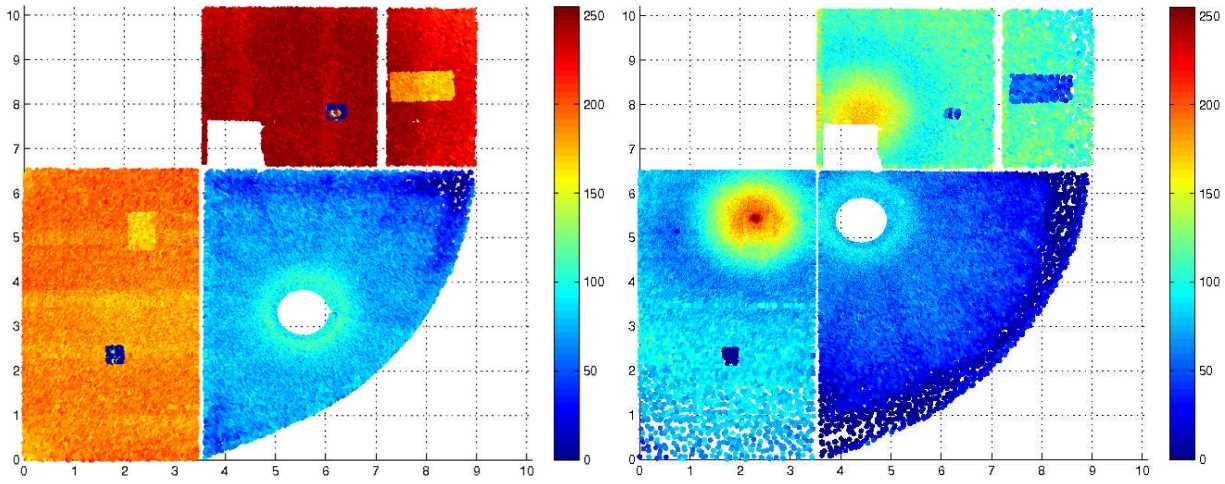
Lindenbergh, R., Pfeifer, N. and Rabbani, T., 2005. Accuracy Analysis of the Leica HDS3000 and feasibility of tunnel deformation monitoring. In: Proceedings of the ISPRS Workshop, Laser scanning 2005, Vol. XXXVI(3/W3), Enschede, The Netherlands, pp. 24–29.

Pfeifer, N., Dorninger, P., Haring, A. and Fan, H., 2007. Investigating terrestrial laser scanning intensity data: quality and functional relations. In: Proceedings International Conference on Optical 3-D Measurement Techniques VIII, Zurich, Switzerland.

Soudarissanane, S., Van Ree, J., Bucksch, A. and Lindenbergh, R., 2007. Error budget of terrestrial laser scanning: influence of the incidence angle on the scan quality. In: Proceedings 3D-NordOst 2007, Berlin, Germany.

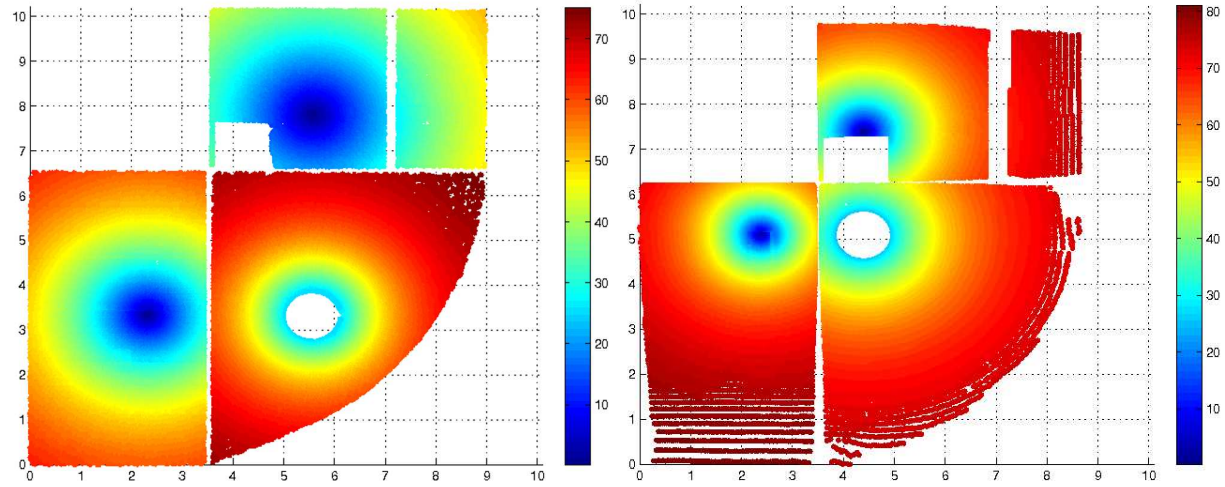
Teunissen, P., 1991. An integrity and quality control procedure for use in multi sensor integration. In: Proceedings of ION GPS-90, Colorado Springs,USA, pp. 513–522.

Zhuang, H. and Roth, Z. S., 1995. Modeling gimbal axis misalignments and mirror center offset in a single-beam laser tracking measurement system. The International Journal of Robotics Research 14(3), pp. 211–224.



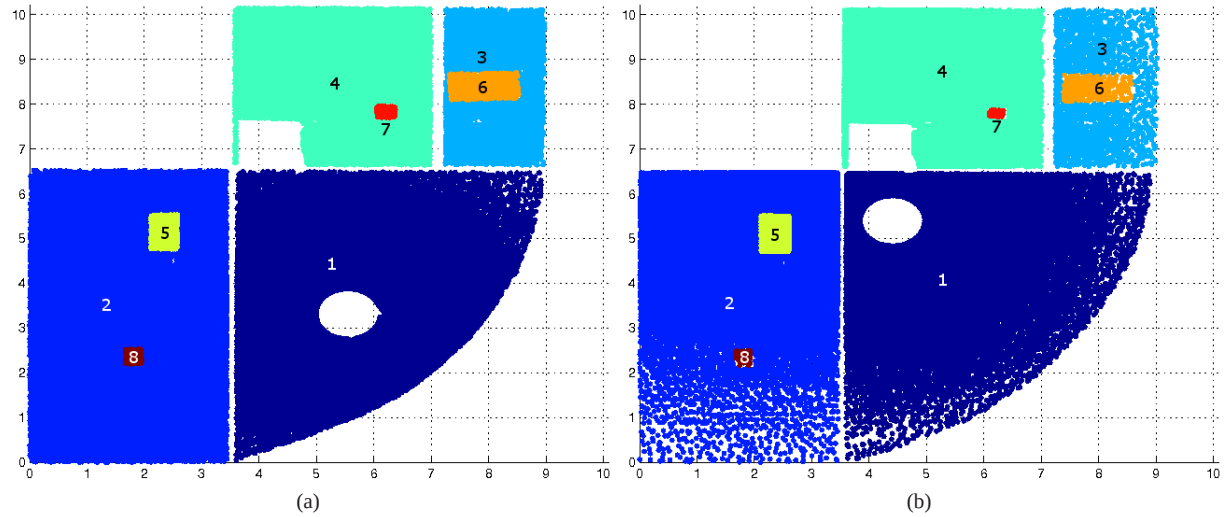
(a) (b)

Figure 2: Intensity.



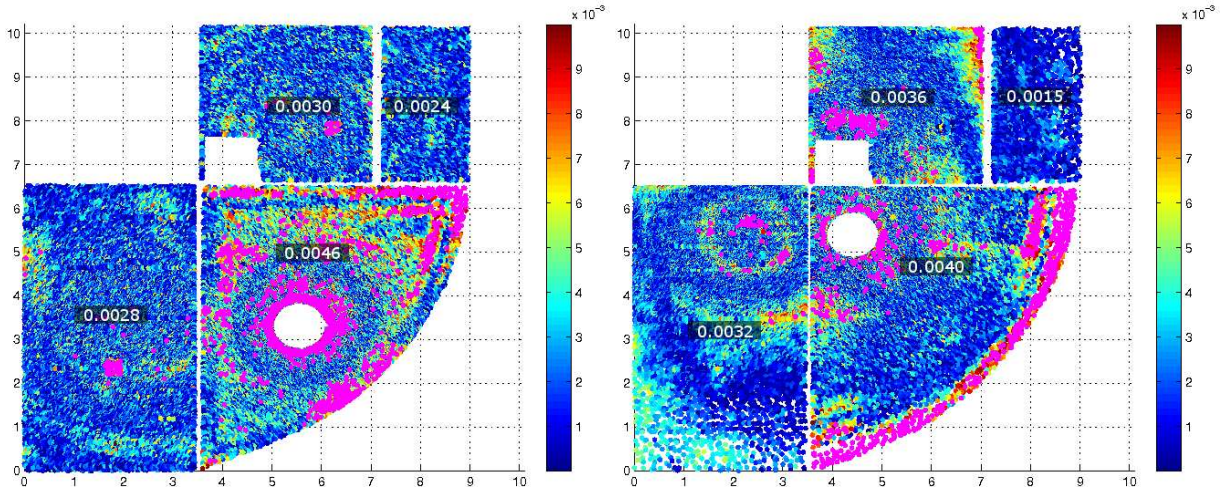
(a) (b)

Figure 3: Incidence angles.



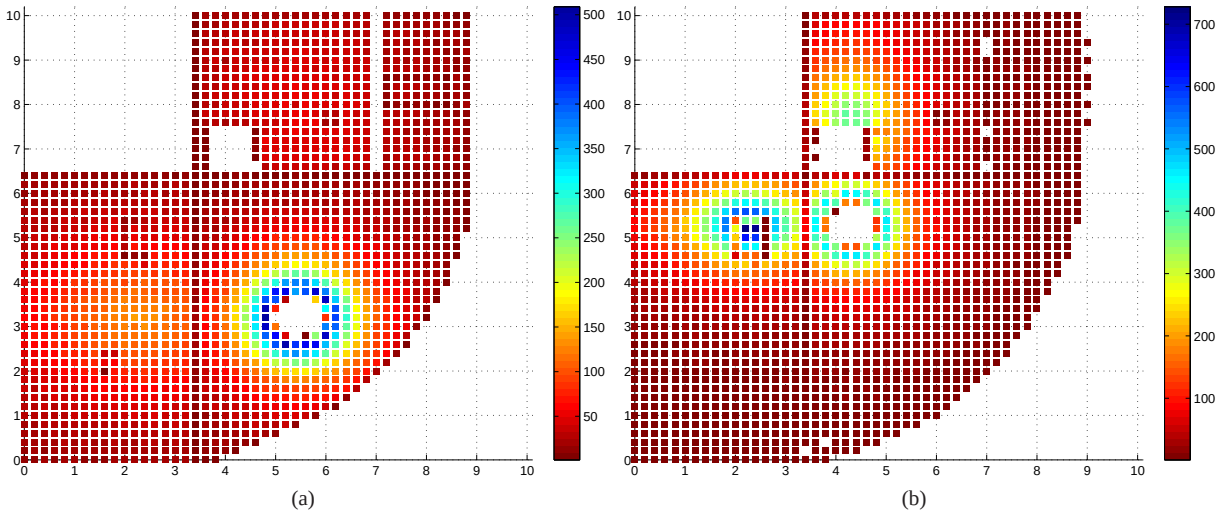

(a) (b)

Figure 4: Segments.



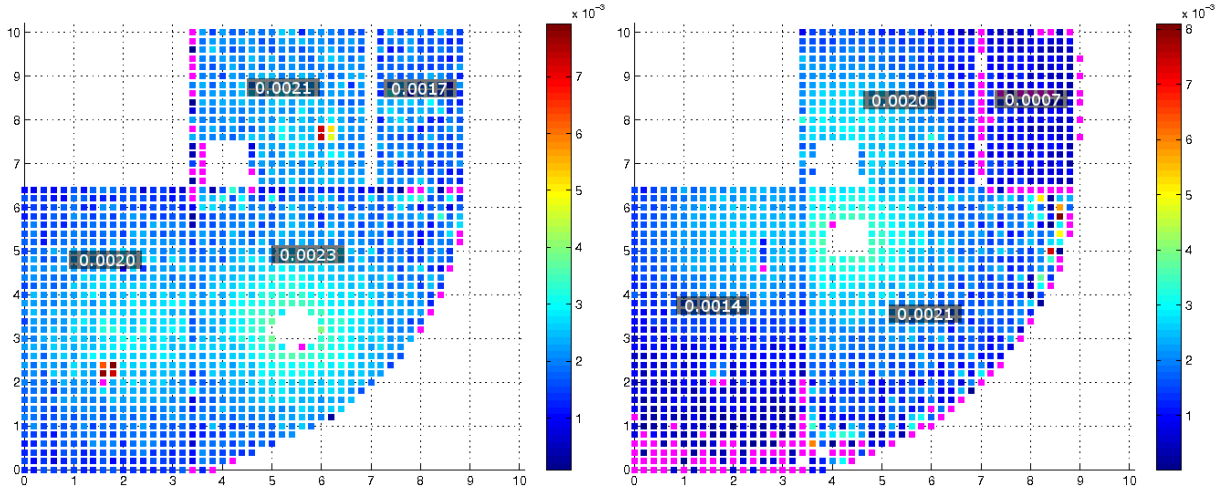

(a) (b)

Figure 5: Individual point residuals w.r.t the eight segments of Fig.4. In the four largest segments, the RMSE of each segment is plotted.



(a) (b)

Figure 6: Number of points per patch of 20 $\times$20 cm.




(a) (b)

Figure 7: Individual patch quality, $\hat{\sigma}_m$, per patch. For the four largest segments, the mean individual patch quality is plotted.